

---

# DEEP KOOPMAN LEARNING OF NONLINEAR TIME-VARYING SYSTEMS

---

**Wenjian Hao**

School of Aeronautics and Astronautics Engineering  
Purdue University, IN, USA  
hao93@purdue.edu

**Bowen Huang**

Pacific Northwest National Laboratory  
Richland, USA  
bowen.h@pnnl.gov

**Wei Pan**

Department of Computer Science  
University of Manchester, UK  
wei.pan@tudelft.nl

**Di Wu**

Pacific Northwest National Laboratory  
Richland, USA  
di.wu@pnnl.gov

**Shaoshuai Mou**

School of Aeronautics and Astronautics Engineering  
Purdue University, IN, USA  
mous@purdue.edu

April 7, 2023

## ABSTRACT

This paper presents a data-driven approach to approximate the dynamics of a nonlinear time-varying system (NTVS) by a linear time-varying system (LTVS), which is resulted from the Koopman operator and deep neural networks. Analysis of the approximation error between states of the NTVS and the resulting LTVS is presented. Simulations on a representative NTVS show that the proposed method achieves small approximation errors, even when the system changes rapidly. Furthermore, simulations in an example of quadcopters demonstrate the computational efficiency of the proposed approach.

## 1 Introduction

In recent years, data-driven methods have received a significant amount of research attention due to the increasing complexity of autonomous system in both dynamics [1–4] and mission objectives [?, ?, ?]. In the direction of learning system dynamics, the Koopman operator has recently been proved to be an effective method to approximate a nonlinear system by a linear time-varying system based on state-control pairs [2–4]. Along this direction, two popular methods dynamic mode decomposition (DMD) and extended dynamic mode decomposition (EDMD) are used to lift the state space to a higher-dimensional space, where the evolution is approximately linear [5]. However, choosing the proper observable functions for the lifting transformation is still an open question, and the potentially large lifted dimension may hinder real-time applications.

Recent work has proposed several methods for choosing proper observable functions of Koopman-based methods for time-invariant systems. Lusch et al. [6] proposed applying deep learning methods to discover the eigenfunctions of the approximated Koopman operator. Yeung et al. [7–10] introduced deep neural networks (DNN) as observable functions of the Koopman operator, which are tuned based on collected state-control pairs by minimizing a properly defined loss function. While some work, such as [11], has extended the DMD method to approximate nonlinear time-varying systems (NTVS) that change sufficiently slowly by linear time-varying systems (LTVS), this method is not directly applicable to approximate nonlinear systems with rapidly changing dynamics.

In this paper, we propose a deep Koopman learning method to approximate NTVS, which employs DNN as the observable function of the Koopman operator and adjusts both the DNN and the approximated dynamical system simultaneously. This is achieved by tuning the DNN parameters based on the latest state-control data pairs to track the unknown NTVS. Compared to existing results in [11], the proposed method is able to approximate an NTVS which does not necessarily to change slowly. Contributions of this paper are summarized as follows:

- We propose a deep Koopman representation formulation for the NTVS and provide a practical online algorithm for implementation.
- We investigate the error bound of the system state estimation of the proposed method.
- We perform a convergence analysis of the proposed method concerning the observable function of DNN.

This paper is organized as follows. In Section 2, we state the problem. Section 3 presents the main results. The numerical simulations are exhibited in Section 4. Finally, Section 5 concludes the paper.

*Notations.* Let  $\|\cdot\|$  denote the Euclidean norm. For a matrix  $A \in \mathbb{R}^{n \times m}$ ,  $\|A\|_F$  denotes its Frobenius norm;  $A^T$  denotes its transpose;  $A^\dagger$  denotes its Moore-Penrose pseudoinverse. For positive integers  $n$  and  $m$ ,  $\mathbf{I}_n$  denotes the  $n \times n$  identity matrix;  $\mathbf{0}_n \in \mathbb{R}^n$  denotes a vector with all value 0;  $\mathbf{0}_{n \times m}$  denotes a  $n \times m$  matrix with all value 0.  $\text{sgn}(\cdot)$  denotes the sign function.  $\lceil \cdot \rceil$  denotes the ceiling function, i.e., given real numbers  $y$ , integers  $k$  and the set of integers  $\mathbb{Z}$ ,  $\lceil y \rceil = \min\{k \in \mathbb{Z} \mid k \geq y\}$ .

## 2 Problem Formulation

Consider an NTVS, the dynamics of which is unknown. Let  $x_t \in \mathbb{R}^n$  and  $u_t \in \mathbb{R}^m$  denote its state and control input at time  $t$ , respectively. Here,  $t \in \mathcal{T}$  with

$$\mathcal{T} = \begin{cases} [0, \infty), & \text{if the NTVS is in continuous-time,} \\ \{0, 1, 2, \dots\}, & \text{if the NTVS is in discrete-time.} \end{cases}$$

Suppose one only observes the unknown NTVS' states and control inputs at certain sampling time instances, as denoted by the following series of data batches

$$\mathcal{B}_\tau = \{x_t, u_t : t \in t_{\mathbb{K}_\tau}\}, \quad \tau = 0, 1, 2, \dots \quad (1)$$

Here,  $t_{\mathbb{K}_\tau} = \{t_{k_\tau}, t_{k_\tau+1}, t_{k_\tau+2}, \dots, t_{k_\tau+\beta_\tau}\} \subset \mathcal{T}$  denotes the ordered set of sampling time instances for the  $\tau$ -th data batch  $\mathcal{B}_\tau$ , where  $\mathbb{K}_\tau = \{k_\tau, k_\tau+1, k_\tau+2, \dots, k_\tau+\beta_\tau\}$ ,  $\tau = 0, 1, 2, \dots$  with  $\beta_\tau$  positive integers such that

$$k_\tau = \sum_{i=0}^{\tau-1} \beta_i, \quad \tau \geq 1, \quad k_0 = 0.$$

It follows that  $k_{\tau+1} = k_\tau + \beta_\tau$ ,  $\tau = 0, 1, 2, \dots$ , which implies the last data in the  $\tau$ th data batch is the first data in  $(\tau+1)$ th data batch. For brevity, one defines  $\mathcal{B}_\tau^x := \{x_t : t \in t_{\mathbb{K}_\tau}\}$ ,  $\mathcal{B}_\tau^u := \{u_t : t \in t_{\mathbb{K}_\tau}\}$  and  $x_{k_\tau} := x_{t_{k_\tau}}$ ,  $u_{k_\tau} := u_{t_{k_\tau}}$  in the remainder of this manuscript.

This paper aims to develop an iterative method that approximates the dynamics of an unknown NTVS based on available data batches  $\mathcal{B}_\tau$  by a linear time-varying discrete-time system. One way to achieve such a linear approximation is by employing the Koopman operator as in [7–10]. Namely, based on the data batch  $\mathcal{B}_\tau$ , one finds a nonlinear mapping  $g(\cdot, \theta_\tau) : \mathbb{R}^n \rightarrow \mathbb{R}^r$  parameterized by  $\theta_\tau \in \mathbb{R}^q$ <sup>1</sup> and matrices  $A_\tau \in \mathbb{R}^{r \times r}$ ,  $B_\tau \in \mathbb{R}^{r \times m}$ ,  $C_\tau \in \mathbb{R}^{n \times r}$  such that for  $k \in \mathbb{K}_\tau$ ,  $k < k_\tau + \beta_\tau$ , the following holds approximately,

$$g(x_{k+1}, \theta_\tau) = A_\tau g(x_k, \theta_\tau) + B_\tau u_k, \quad (2)$$

$$x_{k+1} = C_\tau g(x_{k+1}, \theta_\tau). \quad (3)$$

Here,  $g(\cdot, \theta_\tau)$ ,  $A_\tau$ ,  $B_\tau$ ,  $C_\tau$  achieved from  $\mathcal{B}_\tau$  are put together in the following  $\mathcal{K}_{\mathcal{B}_\tau}$ :

$$\mathcal{K}_{\mathcal{B}_\tau} := \{g(\cdot, \theta_\tau), A_\tau, B_\tau, C_\tau\}, \quad (4)$$

which is called a deep Koopman representation (DKR) in this manuscript.

Based on the DKR in (4), one could introduce  $\hat{x}_k \in \mathbb{R}^n$  for  $k \in \mathbb{K}_\tau$ ,  $k < k_\tau + \beta_\tau$  as followings:

$$g(\hat{x}_{k+1}, \theta_\tau) = A_\tau g(\hat{x}_k, \theta_\tau) + B_\tau \hat{u}_k, \quad (5)$$

$$\hat{x}_{k+1} = C_\tau g(\hat{x}_{k+1}, \theta_\tau), \quad (6)$$

<sup>1</sup>Here,  $g(\cdot, \theta_\tau)$  is usually represented by a DNN with a known structure  $g$  but an adjustable parameter  $\theta_\tau \in \mathbb{R}^q$ .

where

$$\hat{u}_k = u_k, \forall k \in \mathbb{K}_\tau, k < k_\tau + \beta_\tau, \quad \hat{x}_{k_\tau} = x_{k_\tau}. \quad (7)$$

This leads to the following linear system

$$\hat{x}_{k+1} = \hat{A}_\tau \hat{x}_k + \hat{B}_\tau \hat{u}_k, \quad k \in \mathbb{K}_\tau, k < k_\tau + \beta_\tau, \quad (8)$$

with  $\hat{A}_\tau = C_\tau A_\tau C_\tau^\dagger$ ,  $\hat{B}_\tau = C_\tau B_\tau$  and initial conditions in (7). The system (8) can be looked at as a linear approximation to the NTVS based on the data batch  $\mathcal{B}_\tau$ .

To sum up, the **problem of interest** is to develop an iterative update rule to achieve a DKR in (4) based on data batch  $\mathcal{B}_\tau$  in (1) such that the linear system (8) is a nice approximation of the unknown NTVS, i.e.  $\hat{x}_k$  (8) is close to  $x_k$  observed in  $\mathcal{B}_\tau$  from the unknown NTVS in the sense that for any given accuracy  $\varepsilon \geq 0$ ,  $\hat{u}_k = u_k$  and  $\hat{x}_{k_\tau} = x_{k_\tau}$ , the estimation error  $\|\hat{x}_k - x_k\| \leq \varepsilon$ .

### 3 Main Results

This section proposes an algorithm to achieve a deep Koopman representation (DKR) that can approximate an unknown NTVS. We then investigate the estimation error between the state obtained from this DKR, as given in (8), and the observed state of the unknown NTVS.

#### 3.1 Key Idea

Motivated by deep Koopman operator-based methods developed in [7–10], an optimal  $\theta_\tau$  for the deep Koopman representation (DKR), denoted by  $\theta_\tau^*$ , can be obtained by solving the following optimization problem based on the data batch  $\mathcal{B}_\tau$ :

$$\theta_\tau^* = \arg \min_{\theta_\tau \in \mathbb{R}^q} \{w \mathbf{L}_1(A_\tau, B_\tau, \theta_\tau) + (1-w) \mathbf{L}_2(C_\tau, \theta_\tau)\}, \quad (9)$$

where

$$\mathbf{L}_1(A_\tau, B_\tau, \theta_\tau) = \frac{1}{\beta_\tau} \sum_{k=k_\tau}^{k_\tau+\beta_\tau-1} \|g(x_{k+1}, \theta_\tau) - (A_\tau g(x_k, \theta_\tau) + B_\tau u_k)\|^2 \quad (10)$$

and

$$\mathbf{L}_2(C_\tau, \theta_\tau) = \frac{1}{\beta_\tau} \sum_{k=k_\tau}^{k_\tau+\beta_\tau-1} \|x_k - C_\tau g(x_k, \theta_\tau)\|^2. \quad (11)$$

The objectives of (10) and (11) are to approximate (2) and (3), respectively. Here,  $0 < w < 1$  is a constant that combines the objective of minimizing  $\mathbf{L}_1$  and  $\mathbf{L}_2$ . In simple terms,  $\mathbf{L}_1$  and  $\mathbf{L}_2$  measure the simulation errors in the lifted and original coordinates, respectively.

To solve (9), one needs to rewrite the available data batch and objective functions  $\mathbf{L}_1$  and  $\mathbf{L}_2$  in compact forms. Toward this end, the following notation is introduced:

$$\begin{aligned} \mathbf{X}_\tau &= [x_{k_\tau}, x_{k_\tau+1}, \dots, x_{k_\tau+\beta_\tau-1}] \in \mathbb{R}^{n \times \beta_\tau}, \\ \bar{\mathbf{X}}_\tau &= [x_{k_\tau+1}, x_{k_\tau+2}, \dots, x_{k_\tau+\beta_\tau}] \in \mathbb{R}^{n \times \beta_\tau}, \\ \mathbf{U}_\tau &= [u_{k_\tau}, u_{k_\tau+1}, \dots, u_{k_\tau+\beta_\tau-1}] \in \mathbb{R}^{m \times \beta_\tau}. \end{aligned}$$

Then  $\mathbf{L}_1$  in (10) and  $\mathbf{L}_2$  in (11) can be rewritten as

$$\mathbf{L}_1 = \frac{1}{\beta_\tau} \|\bar{\mathbf{G}}_\tau - (A_\tau \mathbf{G}_\tau + B_\tau \mathbf{U}_\tau)\|_F^2 \quad (12)$$

and

$$\mathbf{L}_2 = \frac{1}{\beta_\tau} \|\mathbf{X}_\tau - C_\tau \mathbf{G}_\tau\|_F^2, \quad (13)$$

where

$$\begin{aligned} \mathbf{G}_\tau &= [g(x_{k_\tau}, \theta_\tau), \dots, g(x_{k_\tau+\beta_\tau-1}, \theta_\tau)] \in \mathbb{R}^{r \times \beta_\tau}, \\ \bar{\mathbf{G}}_\tau &= [g(x_{k_\tau+1}, \theta_\tau), \dots, g(x_{k_\tau+\beta_\tau}, \theta_\tau)] \in \mathbb{R}^{r \times \beta_\tau}. \end{aligned} \quad (14)$$

By minimizing  $\mathbf{L}_1$  with respect to  $A_\tau, B_\tau$  in (12) and minimizing  $\mathbf{L}_2$  regarding  $C_\tau$  in (13),  $A_\tau, B_\tau, C_\tau$  can be determined by  $\theta_\tau$  as follows:

$$[A_\tau^\theta, B_\tau^\theta] = \bar{\mathbf{G}}_\tau \begin{bmatrix} \mathbf{G}_\tau \\ \mathbf{U}_\tau \end{bmatrix}^\dagger, \quad (15)$$

$$C_\tau^\theta = \mathbf{X}_\tau \mathbf{G}_\tau^\dagger. \quad (16)$$

Replacing  $A_\tau$  and  $B_\tau$  in (10) by (15) and  $C_\tau$  in (11) by (16), the objective function in (9) can be reformulated as

$$\mathbf{L}(\theta_\tau) = \frac{1}{\beta_\tau} \sum_{k=k_\tau}^{k_\tau+\beta_\tau-1} \left\| \begin{bmatrix} g(x_{k+1}, \theta_\tau) \\ x_k \end{bmatrix} - K_\tau^\theta \begin{bmatrix} g(x_k, \theta_\tau) \\ u_k \end{bmatrix} \right\|^2, \quad (17)$$

with

$$K_\tau^\theta = \begin{bmatrix} A_\tau^\theta & B_\tau^\theta \\ C_\tau^\theta & \mathbf{0}_{n \times m} \end{bmatrix}.$$

Applying the existing deep Koopman operator methods developed in [7–10] to achieve the DKR by solving (9) based on each  $\mathcal{B}_\tau$  available has two shortcomings. First, computing the pseudo-inverse in (15) and (16) repeatedly while solving (9) becomes computationally expensive as  $\tau$  increases. Second,  $\theta_\tau$  must be initialized for each  $\mathcal{B}_\tau$ , which can be challenging in time-varying systems applications. To overcome these two limitations, one can apply the deep Koopman operator method to approximate the unknown NTVS efficiently, and we propose the following method.

### 3.2 Algorithm

Before proceeding on, we need the following assumption.

**Assumption 1** The matrix  $\mathbf{G}_\tau \in \mathbb{R}^{r \times \beta_\tau}$  in (14) and  $\begin{bmatrix} \mathbf{G}_\tau \\ \mathbf{U}_\tau \end{bmatrix} \in \mathbb{R}^{(r+m) \times \beta_\tau}$  are of full row rank.

**Remark 1** Assumption 1 is to ensure the matrices  $\mathbf{G}_\tau \in \mathbb{R}^{r \times \beta_\tau}$  and  $\begin{bmatrix} \mathbf{G}_\tau \\ \mathbf{U}_\tau \end{bmatrix} \in \mathbb{R}^{(r+m) \times \beta_\tau}$  invertible and it naturally requires  $\beta_\tau \geq r + m$ .

**Lemma 1** Given  $\mathcal{K}_{\mathcal{B}_\tau}$  in (4), if Assumption 1 holds, then the matrices  $A_{\tau+1}^\theta, B_{\tau+1}^\theta, C_{\tau+1}^\theta$  can be achieved by

$$[A_{\tau+1}^\theta, B_{\tau+1}^\theta] = (\bar{\mathbf{G}}_{\tau+1} - [A_\tau^\theta, B_\tau^\theta] \chi_{\tau+1}) \lambda_\tau \chi_{\tau+1}^T (\chi_\tau \chi_\tau^T)^{-1} + [A_\tau^\theta, B_\tau^\theta], \quad (18)$$

$$C_{\tau+1}^\theta = (\mathbf{X}_{\tau+1} - C_\tau^\theta \mathbf{G}_{\tau+1}) \bar{\lambda}_\tau \mathbf{G}_{\tau+1}^T (\mathbf{G}_\tau \mathbf{G}_\tau^T)^{-1} + C_\tau^\theta, \quad (19)$$

where  $\chi_\tau = \begin{bmatrix} \mathbf{G}_\tau \\ \mathbf{U}_\tau \end{bmatrix} \in \mathbb{R}^{(r+m) \times \beta_\tau}$ ,  $\lambda_\tau = (\mathbf{I}_{\beta_{\tau+1}} + \chi_{\tau+1}^T (\chi_\tau \chi_\tau^T)^{-1} \chi_{\tau+1})^{-1} \in \mathbb{R}^{\beta_{\tau+1} \times \beta_{\tau+1}}$ ,  $\bar{\lambda}_\tau = (\mathbf{I}_{\beta_{\tau+1}} + \mathbf{G}_{\tau+1}^T (\mathbf{G}_\tau \mathbf{G}_\tau^T)^{-1} \mathbf{G}_{\tau+1})^{-1} \in \mathbb{R}^{\beta_{\tau+1} \times \beta_{\tau+1}}$  with  $\mathbf{G}_{\tau+1} \in \mathbb{R}^{r \times \beta_{\tau+1}}$ ,  $\bar{\mathbf{G}}_{\tau+1} \in \mathbb{R}^{r \times \beta_{\tau+1}}$  defined in (14).

The proof of Lemma 1 will be given in Appendix.

To initialize the algorithm, one first needs to build the DNN  $g(\cdot, \theta_\tau) : \mathbb{R}^n \rightarrow \mathbb{R}^r$  with non-zero  $\theta_\tau \in \mathbb{R}^q$ . Then the matrices  $A_\tau^\theta \in \mathbb{R}^{r \times r}$ ,  $B_\tau^\theta \in \mathbb{R}^{r \times m}$  and  $C_\tau^\theta \in \mathbb{R}^{n \times r}$  can be found by solving (15) and (16), respectively, based on  $\mathcal{B}_\tau$ . When the data batch  $\mathcal{B}_{\tau+1}$  becomes available, one can directly update the  $\mathbf{G}_{\tau+1}$  and  $\bar{\mathbf{G}}_{\tau+1}$  by following (14), which leads to the  $\chi_{\tau+1}$ ,  $\lambda_\tau$  and  $\bar{\lambda}_\tau$  in Lemma 1. Thus one can update  $A_\tau^\theta$ ,  $B_\tau^\theta$  and  $C_\tau^\theta$  efficiently by computing (18)-(19) instead of solving (15)-(16) repeatedly as a consequence of applying Lemma 1. Finally, an optimal  $\theta_{\tau+1}^*$  is obtained by solving (9) with  $A_{\tau+1}^\theta, B_{\tau+1}^\theta$  subject to (18) and  $C_{\tau+1}^\theta$  satisfying (19) based on  $\mathcal{B}_{\tau+1}$ .

To sum up, we have the following algorithm, which is referred to as deep Koopman for time-varying systems (DKTV) in the remainder of this manuscript:

1. Initialization: Build  $g(\cdot, \theta_\tau) : \mathbb{R}^n \rightarrow \mathbb{R}^r$  with  $\theta_\tau \in \mathbb{R}^q$ ,  $\theta_\tau \neq \mathbf{0}_q$ ; initialize  $A_\tau^\theta, B_\tau^\theta$  and  $C_\tau^\theta$  by solving (15) and (16), respectively, based on  $\mathcal{B}_\tau$ .
2. When  $\mathcal{B}_{\tau+1}$  becomes available, update  $A_\tau^\theta, B_\tau^\theta$  and  $C_\tau^\theta$  according to (18) and (19), respectively.
3. Solve (9) to find  $\theta_{\tau+1}^*, A_{\tau+1}^{\theta^*}, B_{\tau+1}^{\theta^*}$  and  $C_{\tau+1}^{\theta^*}$ .
4. Repeat steps 2-3 as the unknown NTVS evolves.

### 3.3 Analysis of the Approximation Error

With a slight abuse of notation, suppose one observes the latest  $\mathcal{B}_\tau$  with  $\{x_{k-1}, u_{k-1}\}$  its latest data point (i.e.,  $x_{k-1} := x_{k_\tau + \beta_\tau}$ ,  $u_{k-1} := u_{k_\tau + \beta_\tau}$ ), in this subsection, we investigate the estimation errors induced by the proposed algorithm described as:

$$e_k = \hat{x}_k - x_k, \quad (20)$$

where  $\hat{x}_k \in \mathbb{R}^n$  denotes the estimated state achieved by the proposed method and  $x_k \in \mathbb{R}^n$  denotes the state of the unknown NTVS evolving from  $x_{k-1} \in \mathbb{R}^n$  and  $u_{k-1} \in \mathbb{R}^m$ . Here, to analyze the (20) with respect to  $\theta_\tau \in \mathbb{R}^q$ , one rewrites (5)-(6) as:

$$\hat{x}_k = C_\tau(A_\tau g(\hat{x}_{k-1}, \theta_\tau) + B_\tau \hat{u}_{k-1}), \quad (21)$$

with condition (7) hold.

Before we present the results, the following concepts about operators are introduced.

#### 3.3.1 Preliminaries

**Definition 1 (Koopman operator with control)** Consider the Hilbert space  $\mathcal{F}$  and discrete-time nonlinear time-varying system  $x_{k+1} = f(x_k, u_k, k)$  starting from time  $k_0$ , where  $k \in \mathbb{Z}$  denotes its time index;  $x_k \in \mathcal{M}$  and  $u_k \in \mathcal{U}$  denote the system state and control input at time  $k$ , respectively;  $\mathcal{M} \subseteq \mathbb{R}^n$  and  $\mathcal{U} \subseteq \mathbb{R}^m$  denote the state space and control input space, respectively. Then the dynamics of the states of the augmented control system  $z_k, z_{k+1}$  is described by

$$z_{k+1} = F(z_k, k) := \begin{bmatrix} f(x_k, \mathbf{u}(0), k) \\ \mathbf{S}\mathbf{u} \end{bmatrix},$$

where  $z_k = \begin{bmatrix} x_k \\ \mathbf{u} \end{bmatrix}$  denotes the augmented control system states;  $\mathbf{S}\mathbf{u}$  denotes the left shifting of the control sequence  $\mathbf{u}$ , i.e.,  $(\mathbf{S}\mathbf{u})(i) = \mathbf{u}(i+1)$  and  $\mathbf{u}(i)$  denotes the  $i$ th element of the control sequence  $\mathbf{u}$ .

We then extend the definition of the Koopman operator from [?] to discrete-time NTVS. Let operator  $\mathcal{K}^{(k_0, k)} : \mathcal{F} \rightarrow \mathcal{F}$  act on functions of state space  $\phi(\cdot) \in \mathcal{F}$  with  $\phi(\cdot) : \mathcal{M} \times \mathcal{U} \rightarrow \mathbb{C}$  and defined with two parameters  $(k_0, k)$  as

$$\mathcal{K}^{(k_0, k)}[\phi(z_k)] = \phi(F(z_k, k)).$$

**Definition 2 ( $L_2$ -projection [12])** For brevity, we recall the definitions of  $\mathcal{F}$ ,  $\mathcal{M}$ , and  $\phi(\cdot)$  from Definition 1. Let  $\nu \in \mathbb{R}$  be the positive measurement on  $\mathcal{M}$  and assume that  $\mathcal{F} = L_2(\nu)$ . Given a set of linearly independent  $\phi_i \in \mathcal{F}$  with  $i = 1, 2, \dots, r$ , and define

$$\begin{aligned} \mathcal{F}_r &:= \text{span}\{\phi_1, \phi_2, \dots, \phi_r\}, \\ \Phi_r &= [\phi_1, \phi_2, \dots, \phi_r]^T. \end{aligned}$$

Then for all nonzero  $c \in \mathbb{R}^r$ , the  $L_2(\nu)$  projection of a function  $\psi \in L_2(\nu)$  on  $\mathcal{F}_r$  is defined as

$$\begin{aligned} P_r^\nu \psi &= \arg \min_{f \in \mathcal{F}_r} \|f - \psi\|_{L_2(\nu)} \\ &= \arg \min_{f \in \mathcal{F}_r} \int_{\mathcal{M}} |f - \psi|^2 d\nu \\ &\Rightarrow \arg \min_{c \in \mathbb{R}^r} \int_{\mathcal{M}} |c^\top \Phi_r - \psi|^2 d\nu. \end{aligned}$$

**Definition 3 (Bounded operator)** Given a Hilbert space  $\mathcal{F}$ , an operator  $\mathcal{O} : \mathcal{F} \rightarrow \mathcal{F}$  is bounded on  $\mathcal{F}$  if

$$\|\mathcal{O}\| := \sup_{f \in \mathcal{F}, \|f\|=1} \|\mathcal{O}f\| < \infty.$$

$\|\mathcal{O}\|$  is referred as the operator norm of  $\mathcal{O}$  in the remainder of this manuscript.

**Definition 4 (Strong Convergence of operator)** A sequence of bounded operators  $\mathcal{O}_i : \mathcal{F} \rightarrow \mathcal{F}$  defined on a Hilbert space  $\mathcal{F}$  converges strongly (or in the strong operator topology) to an operator  $\mathcal{O} : \mathcal{F} \rightarrow \mathcal{F}$  if

$$\lim_{i \rightarrow \infty} \|\mathcal{O}_i f - \mathcal{O}f\| = 0$$

for all  $f \in \mathcal{F}$ .

### 3.3.2 Analysis

We make the following assumptions to show that the error  $e_k$  in (20) is bounded.

**Assumption 2** For any  $\mathcal{B}_\tau$  in (1), let  $\{x_i, u_i\}$  denote its  $i$ th data point observed at time  $t_i$ . The observation interval  $\Delta t = t_{i+1} - t_i$  is sufficiently small such that for some  $\mu_x \geq 0, \mu_u \geq 0, \|x_{i+1} - x_i\| < \mu_x < \infty$  and  $\|u_{i+1} - u_i\| < \mu_u < \infty$ .

**Assumption 3** The deep neural network observable function  $g(\cdot, \theta_\tau)$  is Lipschitz continuous on the system state space with Lipschitz constant  $\mu_g$ .

Consider a DNN observable function  $g(\cdot, \theta_\tau) : \mathbb{R}^n \rightarrow \mathbb{R}^r$ , let  $\bar{\psi}^h = [\bar{\psi}_1^h, \bar{\psi}_2^h, \dots, \bar{\psi}_{n_h}^h]^T \in \mathbb{R}^{n_h}$  be its last hidden layer and  $\bar{\psi}^o = [\bar{\psi}_1^o, \bar{\psi}_2^o, \dots, \bar{\psi}_r^o]^T \in \mathbb{R}^r$  denotes its output layer, where  $\bar{\psi}_i^h : \mathbb{R} \rightarrow \mathbb{R}$  and  $\bar{\psi}_i^o : \mathbb{R} \rightarrow \mathbb{R}$  are generally nonlinear function chosen by user. For simplicity, let  $g_{\theta_\tau}^N$  be a DNN with its last hidden layer containing  $N$  nodes.

**Assumption 4** (1): Given a Hilbert space  $\mathcal{F}$ , the Koopman operator  $\mathcal{K}$  is bounded and continuous on  $\mathcal{F}$ ; (2):  $\bar{\psi}^h$  are selected from the orthonormal basis of  $\mathcal{F}$ , i.e.,  $[\bar{\psi}_1^h, \bar{\psi}_2^h, \dots, \bar{\psi}_\infty^h]^T$  is an orthonormal basis of  $\mathcal{F}$ .

**Remark 2** Since  $g_{\theta_\tau}^N$  is with known structure, one can make Assumption 4 hold by choosing proper activation functions for DNN's different layers. We refer to [13] for more details about candidate functions like the radial basis function.

**Lemma 2** Let  $\mu \in \mathbb{R}$  be the empirical measurements associated with the observed states  $x_k \in \mathbb{R}^n$ . If Assumption 4 holds, then the operator  $P_{n_h}^\mu$  converges strongly to the identity operator  $I$  as  $n_h$  goes to infinity.

Proof of Lemma 2 is referred to in Appendix.

**Lemma 3** Let  $P := \begin{bmatrix} P_{n_h}^{\mu_1} & \mathbf{0}_{n_h \times m} \\ \mathbf{0}_{m \times n_h} & P_m^{\mu_2} \end{bmatrix}$  with  $\mu_1 \in \mathbb{R}, \mu_2 \in \mathbb{R}$  the empirical measurements associated to the observed system state  $x_k \in \mathbb{R}^n$  and control input  $u_k \in \mathbb{R}^m$ , respectively. If Assumption 4 holds, then the approximated sequence of operators  $\mathcal{K}_D P = P \mathcal{K} P$  converges to Koopman operator  $\mathcal{K}$  strongly as  $n_h$  goes to infinity.

Proof of Lemma 3 is given in Appendix.

**Remark 3** Lemma 3 shows the convergence condition of the existing DKO method regarding the DNN observable function  $g(\cdot, \theta_\tau)$  ( $n_h \rightarrow \infty$ ). It replaces the convergence condition of the EDMD method [12] ( $r \rightarrow \infty$ ). This conclusion is used in the present work to reduce  $\beta_\tau \geq r + m$  so that one can track the unknown NTVS based on  $\mathcal{B}_\tau$  with small batch size.

**Theorem 1** If Assumptions 1-4 hold, then the estimation error  $e_k$  in (20) is bounded by

$$\lim_{n_h \rightarrow \infty} \sup \|e_k\| = (\|C_\tau A_\tau\| \mu_g + 1) \mu_x + \|C_\tau B_\tau\| \mu_u + \max_{\bar{x} \in \mathcal{B}_\tau^z} \|\bar{x} - C_\tau g(\bar{x}, \theta_\tau)\|.$$

The proof of Theorem 1 is given in Appendix.

**Remark 4** Theorem 1 says that with certain assumptions hold, as  $n_h \rightarrow \infty$ , the estimation error of the proposed method depends on the minimization performance of (13) and  $\mu_x, \mu_u$  defined in Assumption 2. One way to further reduce the estimation error is to decrease the sampling interval.

Since one cannot construct a DNN with infinite parameters in practice, we introduce the following corollary based on Theorem 1, for which we need to make the following assumption.

**Assumption 5** For any  $A_\tau \in \mathbb{R}^{r \times r}$ ,  $\|A_\tau\| < 1$ .

**Remark 5** According to Lemma 1, the DNN observable function determines  $\|A_\tau\|$ . To make Assumption 5 hold, one can add an extra loss function to impose the maximum value of  $\|A_\tau\|$  in (9).

**Corollary 1** Recall  $e_k$  in (20). If Assumptions 1-3 and 5 hold, then the upper bound of  $\|e_k\|$  is determined by the minimization performance of (17) and  $\mu_x, \mu_u$  as  $k$  goes to infinity.

The proof of Corollary 1 is given in Appendix.

## 4 Numerical Simulations

In this section, we test the proposed algorithm in two examples, one is a simple nonlinear time-varying system (NTVS), and the other one is aquadcopter. In both examples, the system state input data is observed with a fixed time interval of 0.1s, and  $\beta_\tau \equiv \beta$ , where  $\beta \geq r + m$  is an arbitrary positive integer, and  $\tau = \lceil \frac{k-\beta_0}{\beta} \rceil$ , where  $k \in \mathbb{K}_\tau$ .

### 4.1 A Simple NTVS

Consider the following dynamical system:

$$\dot{x}_t = M_t \cos(x_t), \quad (22)$$

where  $x_t \in \mathbb{R}^2$  and  $M_t$  is a time-varying matrix given by

$$M_t = \begin{bmatrix} 0 & (1 + \gamma t) \\ -(1 + \gamma t) & 0 \end{bmatrix}, \quad (23)$$

where  $\gamma$  is a constant determining how fast the dynamics change. For more details of the dynamics, see [11].

The DNN observable function  $(g(\cdot, \theta) : \mathbb{R}^2 \rightarrow \mathbb{R}^6)$  is built with a hidden layer *Gaussian function* that contains 32 nodes and an output layer *Relu()* consisting of 6 nodes. The DNN training process is implemented by choosing optimizer *Adam* [14] with *learning rate* =  $1e-3$  and *weight decay rate* =  $1e-4$ . Then  $\mathcal{B}_\tau$  is observed with  $\beta = 10$  starting from  $x_0 = [1, 0]^T$ . We test the proposed method in the NTVS in (22) for both slow and fast-changing scenarios setting  $\gamma = 0.8$  and  $\gamma = 6$ , respectively. The trajectories estimated by time-varying DMD(TVDMD) and the proposed method are shown in Figs. 1, and the estimation errors of both methods are exhibited in Fig. 2. Here, we let  $x_k \in \mathbb{R}^2$  denote the true system states observed from the unknown NTVS. Let  $\tilde{x}_k \in \mathbb{R}^2$  denote the estimated states generated by the TVDMD method from [11]. Let  $\hat{x}_k \in \mathbb{R}^2$  be the estimated states from the proposed method (DKTV), as given in (21). Consequently,  $\tilde{e}_k = \|\tilde{x}_k - x_k\|$  and  $e_k = \|\hat{x}_k - x_k\|$  denote the estimation errors induced by the TVDMD and DKTV methods, respectively. It can be observed that when the NTVS varies slowly, both methods can capture

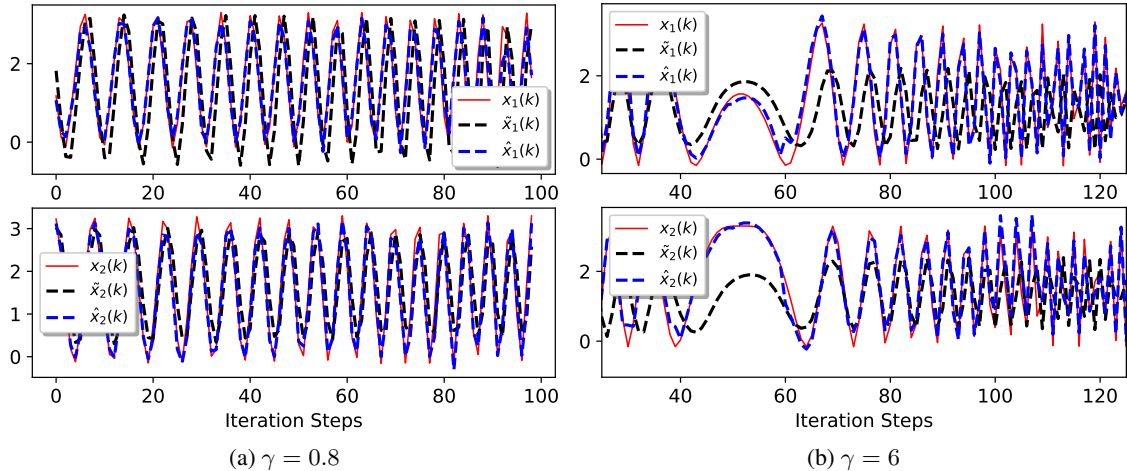


Figure 1: System states trajectories: TVDMD (black) vs. DKTV (blue)

the dynamics of the NTVS with reasonable accuracy. In situations where the NTVS varies rapidly, the estimation errors of the TVDMD method increase correspondingly. On the contrary, the proposed method can achieve consistent performance, benefiting from its DNN observable function.

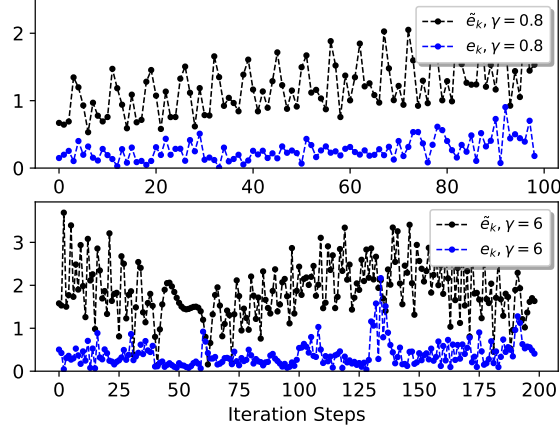


Figure 2: System states estimation errors: TVDMD (black) vs. DKTV (blue)

## 4.2 System States Prediction for Single Quadcopter

In this example, we implement the proposed algorithm to predict the system states of a quadcopter with a time-varying disturbance applied to its body. The dynamics of the quadcopter is described as

$$\begin{aligned} \begin{pmatrix} \dot{p}_n \\ \dot{p}_e \\ \dot{z} \end{pmatrix} &= \begin{pmatrix} c_\theta c_\psi & s_\phi s_\theta c_\psi - c_\phi s_\psi & c_\phi s_\theta c_\psi + s_\phi s_\psi \\ c_\theta c_\psi & s_\phi s_\theta s_\psi + c_\phi c_\psi & c_\phi s_\theta s_\psi - s_\phi c_\psi \\ s_\theta & -s_\phi c_\theta & -c_\phi c_\theta \end{pmatrix} \begin{pmatrix} \dot{x} \\ \dot{y} \\ \dot{z} \end{pmatrix}, \\ \begin{pmatrix} \dot{\phi} \\ \dot{\theta} \\ \dot{\psi} \end{pmatrix} &= \begin{pmatrix} 1 & s_\phi t_\theta & c_\phi t_\theta \\ 0 & c_\phi & -s_\phi \\ 0 & \frac{s_\phi}{c_\theta} & \frac{c_\phi}{s_\theta} \end{pmatrix} \begin{pmatrix} p \\ q \\ r \end{pmatrix}, \\ \begin{pmatrix} \ddot{x} \\ \ddot{y} \\ \ddot{z} \end{pmatrix} &= \begin{pmatrix} r\dot{y} - q\dot{z} \\ p\dot{z} - r\dot{x} \\ q\dot{x} - p\dot{y} \end{pmatrix} + \frac{1}{m} \begin{pmatrix} f_x \\ f_y \\ f_z \end{pmatrix} + w_t, \\ \begin{pmatrix} \dot{p} \\ \dot{q} \\ \dot{r} \end{pmatrix} &= \begin{pmatrix} \frac{J_y - J_z}{J_x} qr \\ \frac{J_z - J_x}{J_y} pr \\ \frac{J_x - J_y}{J_z} pq \end{pmatrix} + \begin{pmatrix} \frac{1}{J_x} \tau_\phi \\ \frac{1}{J_y} \tau_\theta \\ \frac{1}{J_z} \tau_\psi \end{pmatrix}, \end{aligned}$$

where  $s_\theta$ ,  $s_\phi$ ,  $s_\psi$ ,  $c_\theta$ ,  $c_\phi$ ,  $c_\psi$ , and  $t_\theta$  denote  $\sin(\theta)$ ,  $\sin(\phi)$ ,  $\sin(\psi)$ ,  $\cos(\theta)$ ,  $\cos(\phi)$ ,  $\cos(\psi)$ , and  $\tan(\theta)$ , respectively.  $p_n$ ,  $p_e$ , and  $z$  denote the inertial north position, the inertial east position, and the altitude, respectively.  $\dot{x}$ ,  $\dot{y}$ , and  $\dot{z}$  denote the velocity along the x-axis, y-axis, and z-axis, respectively.  $\phi$ ,  $\theta$ , and  $\psi$  denote the roll angle, pitch angle, and yaw angle, respectively, and  $p$ ,  $q$ , and  $r$  denote the roll rate, pitch rate, and yaw rate, respectively.  $f_x$ ,  $f_y$ , and  $f_z$  denote the total force applied to the quadcopter along the x-axis, y-axis, and z-axis, respectively, and  $w_t \in \mathbb{R}^3$  denotes the time-varying disturbance.  $\tau_\phi$ ,  $\tau_\theta$  and  $\tau_\psi$  denote the torque of roll, pitch, and yaw, respectively, while  $J_x$ ,  $J_y$ , and  $J_z$  denote the inertia along the x-axis, y-axis, and z-axis, respectively. For further details on the dynamics of the quadcopter, see [15].

**Experiment Setup.** In order to compare the performance of the proposed algorithm with that of the single neural network method, we let  $x_k \in \mathbb{R}^{12}$  denote the true state of the system,  $\bar{x}_k \in \mathbb{R}^{12}$  and  $\hat{x}_k \in \mathbb{R}^{12}$  denote the estimated states of the single DNN and the proposed method, respectively, and  $\bar{e}_k = \|\bar{x}_k - x_k\|$  and  $e_k = \|\hat{x}_k - x_k\|$  denote the estimation errors of the single DNN and DKTV methods, respectively. The data batch  $\mathcal{B}_\tau$  is collected with  $\beta = 30$  manually controlling the quadcopter from position (0, 0, 0) (meter) to (1, 2, 3) (meter) with the time-varying disturbance force  $w_t \in \mathbb{R}^3$  applied on the quadcopter.  $w_t$  is generated from the standard normal distribution. For the DKTV method, the DNN observable function  $g(\cdot, \theta) : \mathbb{R}^{12} \rightarrow \mathbb{R}^{16}$  is built with one hidden layer *Gaussian function* containing 64 nodes and one output layer *Relu()* consisting of 16 nodes. For the single DNN method, DNN  $N(\cdot, \nu) : \mathbb{R}^{16} \rightarrow \mathbb{R}^{12}$  is built with the same structure as  $g(\cdot, \theta)$ . Then the DNN training process of both methods is implemented by choosing optimizer *Adam* [14] with *learning rate* = 1e-3 and *weight decay rate* = 1e-4. The optimal vector  $\nu \in \mathbb{R}^p$  is found by

$$\nu^* = \arg \min_{\nu \in \mathbb{R}^p} L(\nu) = \arg \min_{\nu \in \mathbb{R}^p} \|N(x_k, u_k, \nu) - x_{k+1}\|, \quad (24)$$

which leads to  $\bar{x}_{k+1} = N(x_k, u_k, \nu^*)$ .

**Results Analysis.** We first show the DNN training process of both methods with  $\tau = 1, \dots, 7$  in Fig. 3, where one epoch denotes one forward and one backward pass through the DNN and  $L(\nu), L(\theta)$  are defined in (24) and (17), respectively. As shown, DKTV needs fewer training epochs to converge and maintains a much lower loss value during the training process than the single DNN method, as expected due to its double minimization of (12)-(13). Then in

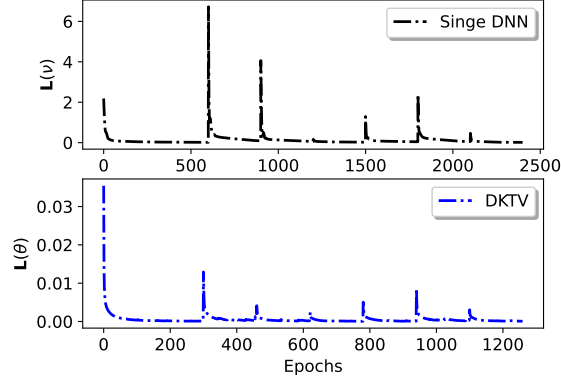


Figure 3: Training process: Single DNN (black) vs. DKTV (blue)

Fig. 4, we demonstrate the algorithm performance by showing the system states estimation errors of both methods. As is shown, the proposed algorithm can provide better prediction performance compared with the Single DNN method. Finally, in Fig. 5, Theorem 1 is validated by showing that the estimation errors of the proposed algorithm are reduced

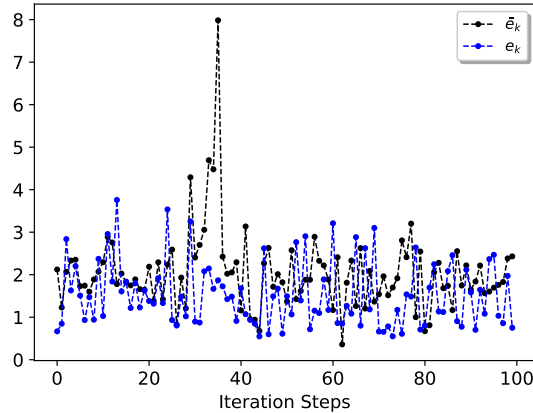


Figure 4: System states estimation error: Single DNN (black) vs. DKTV (blue)

by increasing the number of nodes of its hidden layer.

### 4.3 Optimal Control based on the Proposed Deep Koopman Learning

In this subsection, we design the optimal controller based on the proposed method for a classic cartpole example from [16], where we make the coefficient of friction of cart on track ( $\mu_c(t)$ ) time-varying during the simulation. And we choose the well-studied model predictive control (MPC) method to demonstrate the optimal control application based on the proposed algorithm, of which the optimization problem is formulated as

$$\begin{aligned}
 \min_{u_i, x_i} \quad & J(u_i, x_i) \\
 \text{s.t.} \quad & u_i \in \mathcal{U}, x_i \in \mathcal{X}, i = k_\tau, \dots, k_\tau + \beta_\tau - 1, \\
 & g(x_{i+1}, \theta_\tau) = A_\tau g(x_i, \theta_\tau) + B_\tau u_i, \\
 & x_i = C_\tau g(x_i, \theta_\tau), \\
 & x_{t+l} = x_l,
 \end{aligned} \tag{25}$$

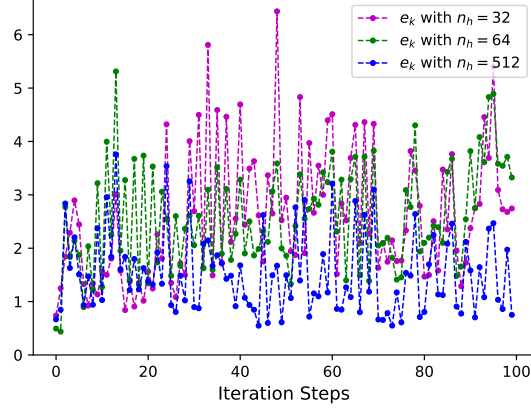


Figure 5: The estimation errors of DKTV with different DNN observable functions

where  $J(u_i, x_i)$  is defined by

$$J(u_i, x_i) = \sum_{i=k_\tau}^{k_\tau+l-1} (\bar{g}(x_i, \theta_\tau)^T \tilde{Q}_\tau \bar{g}(x_i, \theta_\tau) + u_i^T R u_i) + g(x_l, \theta_\tau)^T \tilde{Q}_l g(x_l, \theta_\tau),$$

and  $l \leq \beta_\tau$  is the time horizon;  $i$  is the time-index along the defined time horizon;  $x_i \in \mathbb{R}^n$  and  $u_i \in \mathbb{R}^m$  are the system state and control input at time step  $i$ , respectively;  $\bar{g}(x_i, \theta_\tau) = g(x_i, \theta_\tau) - g(x^*, \theta_\tau)$  with  $x^*$  denoting the goal state;  $x_l$  is the terminal state;  $\mathcal{X}$  denotes the state constraint and  $\mathcal{U}$  denotes the control input constraint;  $\tilde{Q}_\tau = C_\tau^T Q C_\tau \in \mathbb{R}^{r \times r}$ ,  $Q \in \mathbb{R}^{n \times n}$ ,  $R \in \mathbb{R}^{m \times m}$  are positive definite matrices.

### 4.3.1 Time-varying Cartpole Balance

In this example, the physic governing equation of the cartpole is described as

$$\begin{aligned} \ddot{x}_t &= \frac{F_t + ml(\dot{\theta}_t^2 \sin \bar{\theta}_t - \ddot{\theta}_t \cos \bar{\theta}_t) - \mu_t^c \text{sgn}(\dot{x}_t)}{m_c + m} \\ \ddot{\theta}_t &= \frac{\cos \theta_t [-F_t - ml\dot{\theta}_t^2 \sin \theta_t + \mu_t^c \text{sgn}(\dot{x}_t)] / (m_c + m)}{l[\frac{4}{3} - (m \cos^2 \bar{\theta}_t) / (m_c + m)]} \\ &+ \frac{g \sin \theta_t - \mu_p \dot{\theta}_t / ml}{l[\frac{4}{3} - (m \cos^2 \bar{\theta}_t) / (m_c + m)]}, \end{aligned} \quad (26)$$

where  $\mu_t^c = 0.3 \cos(t)$  with  $\mu_0^c = 0.0005$  is the *time-varying* coefficient of friction of cart on track;  $x_t$  denotes the distance of the cartpole moves from the initial position;  $\bar{\theta}_t$  denotes the angle from the up position;  $\dot{x}_t, \dot{\theta}_t$  denote the  $x$ -axis velocity and the angular velocity respectively;  $F_t$  denotes the continuous control input applied to the center of the mass of the cart at time step  $t$ ;  $g = -9.8m/s^2$  is the gravity acceleration;  $m_c = 1.0kg$ ,  $m = 0.1kg$  are the mass of the cart and the pole, respectively;  $l = 0.5m$  is the length of the pole;  $\mu_p = 0.000002$  is the coefficient of the friction of the pole on cart.

For the simulation, we first build the DNN ( $g(\cdot, \theta) : \mathbb{R}^4 \rightarrow \mathbb{R}^6$ ) and set  $\beta = 12$ ; then the  $\mathcal{B}_\tau$  is generated by observing the dynamics in (26) with fixed time interval  $t_{k_\tau+1} - t_{k_\tau} \equiv 0.1s$ . The approximated dynamics is directly applied to design the MPC controller to keep the cartpole balanced at the up position with  $\bar{\theta} = 0, \dot{\bar{\theta}} = 0$ .

*Results Analysis:* Fig. 6 shows the trajectory of the time-varying cartpole under the MPC control based on the proposed method. From the result, the cartpole is able to keep the desired up position under the DKTV-based MPC control even though  $\mu_k^c$  increases from 0.0005 to 14.288.

**Remark 6** In this subsection, we show the MPC design based on approximated linear dynamics from the proposed algorithm. Compared to the existing MPC method for the NTVS proposed in [17–19], the proposed method requires neither the priori knowledge of the system dynamics nor the distribution information of the system disturbance.

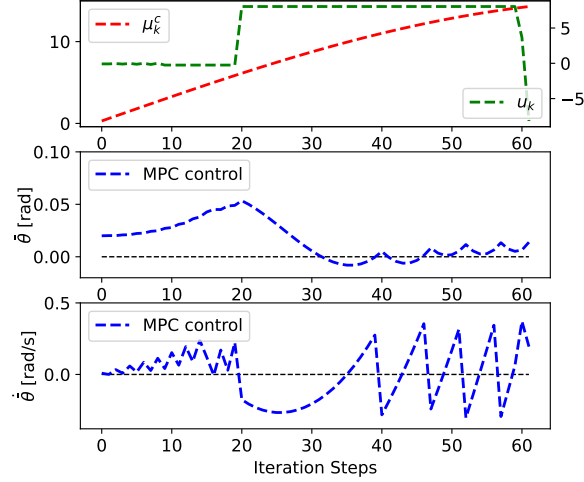


Figure 6: MPC based on the Approximated Dynamics

## 5 Conclusions

This paper presents a data-driven approach to approximate the dynamics of a nonlinear time-varying system (NTVS) by a linear time-varying system (LTVS), which is resulted from the Koopman operator and deep neural networks. The proposed algorithm is able to approximate well a NTVS by iterative update its linear approximation as validated by a simple NTVS system in two dimension. Moreover, controllers developed based on the linear approximation perform well in controlling a quadrotor with complex dynamics. Future work includes employing the proposed method to achieve adaptive autonomy in [?, ?] and to serve as robot's dynamics estimation in human-robot teaming [?, ?].

## References

- [1] Giorgos Mamakoukas, Maria L Castano, Xiaobo Tan, and Todd D Murphey. Derivative-based koopman operators for real-time control of robotic systems. *IEEE Transactions on Robotics*, 37(6):2173–2192, 2021.
- [2] Igor Mezić. On applications of the spectral theory of the koopman operator in dynamical systems and control theory. In *2015 54th IEEE Conference on Decision and Control (CDC)*, pages 7034–7041. IEEE, 2015.
- [3] Joshua L Proctor, Steven L Brunton, and J Nathan Kutz. Generalizing koopman theory to allow for inputs and control. *SIAM Journal on Applied Dynamical Systems*, 17(1):909–930, 2018.
- [4] Alexandre Mauroy and Jorge Goncalves. Linear identification of nonlinear systems: A lifting technique based on the koopman operator. In *2016 IEEE 55th Conference on Decision and Control (CDC)*, pages 6500–6505. IEEE, 2016.
- [5] Milan Korda and Igor Mezić. Linear predictors for nonlinear dynamical systems: Koopman operator meets model predictive control. *Automatica*, 93:149–160, 2018.
- [6] Bethany Lusch, Steven L Brunton, and J Nathan Kutz. Data-driven discovery of koopman eigenfunctions using deep learning. *Bulletin of the American Physical Society*, 2017.
- [7] Enoch Yeung, Soumya Kundu, and Nathan Hodas. Learning deep neural network representations for koopman operators of nonlinear dynamical systems. In *2019 American Control Conference (ACC)*, pages 4832–4839. IEEE, 2019.
- [8] Bethany Lusch, J Nathan Kutz, and Steven L Brunton. Deep learning for universal linear embeddings of nonlinear dynamics. *Nature communications*, 9(1):1–10, 2018.
- [9] Yiqiang Han, Wenjian Hao, and Umesh Vaidya. Deep learning of koopman representation for control. In *2020 59th IEEE Conference on Decision and Control (CDC)*, pages 1890–1895. IEEE, 2020.
- [10] Petar Bevanda, Max Beier, Sebastian Kerz, Armin Lederer, Stefan Sosnowski, and Sandra Hirche. Koopmanizingflows: Diffeomorphically learning stable koopman operators. *arXiv preprint arXiv:2112.04085*, 2021.
- [11] Hao Zhang, Clarence W Rowley, Eric A Deem, and Louis N Cattafesta. Online dynamic mode decomposition for time-varying systems. *SIAM Journal on Applied Dynamical Systems*, 18(3):1586–1609, 2019.

- [12] Milan Korda and Igor Mezić. On convergence of extended dynamic mode decomposition to the koopman operator. *Journal of Nonlinear Science*, 28(2):687–710, 2018.
- [13] Matthew O Williams, Ioannis G Kevrekidis, and Clarence W Rowley. A data-driven approximation of the koopman operator: Extending dynamic mode decomposition. *Journal of Nonlinear Science*, 25(6):1307–1346, 2015.
- [14] Diederik P Kingma and Jimmy Ba. Adam: A method for stochastic optimization. *arXiv preprint arXiv:1412.6980*, 2014.
- [15] Randal W Beard. Quadrotor dynamics and control. *Brigham Young University*, 19(3):46–56, 2008.
- [16] Andrew G Barto, Richard S Sutton, and Charles W Anderson. Neuronlike adaptive elements that can solve difficult learning control problems. *IEEE transactions on systems, man, and cybernetics*, (5):834–846, 1983.
- [17] Marko Tanaskovic, Lorenzo Fagiano, and Vojislav Gligorovski. Adaptive model predictive control for linear time varying mimo systems. *Automatica*, 105:237–245, 2019.
- [18] Pornchai Bumroongsri. Tube-based robust mpc for linear time-varying systems with bounded disturbances. *International Journal of Control, Automation and Systems*, 13(3):620–625, 2015.
- [19] Paolo Falcone, Manuela Tufo, Francesco Borrelli, Jahan Asgari, and H Eric Tseng. A linear time varying model predictive control approach to the integrated vehicle dynamics control problem in autonomous systems. In *2007 46th IEEE Conference on Decision and Control*, pages 2980–2985. IEEE, 2007.
- [20] Giorgos Mamakoukas, Ian Abraham, and Todd D Murphey. Learning data-driven stable koopman operators. *arXiv preprint arXiv:2005.04291*, 2020.

## 6 Appendix

**Proof of Lemma 1.** Similar to the EDMD, we start from solving the least square problem with collected state-control pairs  $\mathcal{B}_\tau$  in (1) and for writing simplicity, let  $x_{k_\tau} := x_{t_{k_\tau}} \in \mathbb{R}^n$  and  $u_{k_\tau} := u_{t_{k_\tau}} \in \mathbb{R}^m$ .

$$\begin{aligned}\mathbf{X}_\tau &= [x_{k_\tau}, x_{k_\tau+1}, \dots, x_{k_\tau+\beta_\tau-1}] \in \mathbb{R}^{n \times \beta_\tau}, \\ \bar{\mathbf{X}}_\tau &= [x_{k_\tau+1}, x_{k_\tau+2}, \dots, x_{k_\tau+\beta_\tau}] \in \mathbb{R}^{n \times \beta_\tau}, \\ \mathbf{U}_\tau &= [u_{k_\tau}, u_{k_\tau+1}, \dots, u_{k_\tau+\beta_\tau-1}] \in \mathbb{R}^{m \times \beta_\tau}.\end{aligned}$$

Given  $g(\cdot, \theta_\tau) : \mathbb{R}^n \rightarrow \mathbb{R}^r$  with fixed vector  $\theta_\tau \in \mathbb{R}^q$ , matrices  $A_\tau \in \mathbb{R}^{r \times r}$ ,  $B_\tau \in \mathbb{R}^{r \times m}$  are obtained by solving

$$\min_{A_\tau \in \mathbb{R}^{r \times r}, B_\tau \in \mathbb{R}^{r \times m}} \|\bar{\mathbf{G}}_\tau - A_\tau \mathbf{G}_\tau - B_\tau \mathbf{U}_\tau\|_F^2,$$

of which the unique minimum-norm solution is given by

$$[A_\tau^\theta, B_\tau^\theta] = \bar{\mathbf{G}}_\tau \begin{bmatrix} \mathbf{G}_\tau \\ \mathbf{U}_\tau \end{bmatrix}^\dagger, \quad (27)$$

where  $\mathbf{G}_\tau \in \mathbb{R}^{r \times \beta_\tau}$ ,  $\bar{\mathbf{G}}_\tau \in \mathbb{R}^{r \times \beta_\tau}$  are defined in (14). Set

$$\begin{aligned}V_\tau &= \bar{\mathbf{G}}_\tau \begin{bmatrix} \mathbf{G}_\tau \\ \mathbf{U}_\tau \end{bmatrix}^T, G_\tau = \begin{bmatrix} \mathbf{G}_\tau \\ \mathbf{U}_\tau \end{bmatrix} \begin{bmatrix} \mathbf{G}_\tau \\ \mathbf{U}_\tau \end{bmatrix}^T, \\ M_\tau &= [A_\tau^\theta, B_\tau^\theta],\end{aligned}$$

then (27) is rewritten as  $M_\tau = V_\tau G_\tau^{-1}$ . As we obtain new state-control data pairs denoted by  $\mathbf{X}_{\tau+1}$ ,  $\bar{\mathbf{X}}_{\tau+1}$  and  $\mathbf{U}_{\tau+1}$ , matrices  $V_{\tau+1}$ ,  $G_{\tau+1}$  are updated by

$$\begin{aligned}V_{\tau+1} &= [\bar{\mathbf{G}}_\tau \quad \bar{\mathbf{G}}_{\tau+1}] \begin{bmatrix} \mathbf{G}_\tau & \mathbf{G}_{\tau+1} \\ \mathbf{U}_\tau & \mathbf{U}_{\tau+1} \end{bmatrix}^T \\ &= V_\tau + \bar{\mathbf{G}}_{\tau+1} \begin{bmatrix} \mathbf{G}_{\tau+1} \\ \mathbf{U}_{\tau+1} \end{bmatrix}^T,\end{aligned}$$

and

$$\begin{aligned}G_{\tau+1} &= \begin{bmatrix} \mathbf{G}_\tau & \mathbf{G}_{\tau+1} \\ \mathbf{U}_\tau & \mathbf{U}_{\tau+1} \end{bmatrix} \begin{bmatrix} \mathbf{G}_\tau & \mathbf{G}_{\tau+1} \\ \mathbf{U}_\tau & \mathbf{U}_{\tau+1} \end{bmatrix}^T \\ &= G_\tau + \begin{bmatrix} \mathbf{G}_{\tau+1} \\ \mathbf{U}_{\tau+1} \end{bmatrix} \begin{bmatrix} \mathbf{G}_{\tau+1} \\ \mathbf{U}_{\tau+1} \end{bmatrix}^T.\end{aligned} \quad (28)$$

According to the Sherman–Morrison formula:

$$(A + uv^T)^{-1} = A^{-1} - \frac{A^{-1}uv^T A^{-1}}{\mathbf{I} + v^T A^{-1}u},$$

one has:

$$\begin{aligned}M_{\tau+1} &= (V_\tau + \bar{\mathbf{G}}_{\tau+1} \chi_{\tau+1}^T)(G_\tau^{-1} - (G_\tau^{-1} \chi_{\tau+1} \chi_{\tau+1}^T G_\tau^{-1}) \\ &\quad (\mathbf{I}_{\beta_{\tau+1}} + \chi_{\tau+1}^T G_\tau^{-1} \chi_{\tau+1})^{-1}) \\ &= M_\tau - \lambda_\tau M_\tau \chi_{\tau+1} \chi_{\tau+1}^T G_\tau^{-1} \\ &\quad + \lambda_\tau \bar{\mathbf{G}}_{\tau+1} (\lambda_\tau^{-1} - \chi_{\tau+1}^T G_\tau^{-1} \chi_{\tau+1}) \chi_{\tau+1}^T G_\tau^{-1} \\ &= M_\tau - \lambda_\tau M_\tau \chi_{\tau+1} \chi_{\tau+1}^T G_\tau^{-1} \\ &\quad + \lambda_\tau \bar{\mathbf{G}}_{\tau+1} \chi_{\tau+1}^T G_\tau^{-1} \\ &= M_\tau + (\bar{\mathbf{G}}_{\tau+1} - M_\tau \chi_{\tau+1}) \lambda_\tau \chi_{\tau+1}^T G_\tau^{-1},\end{aligned}$$

where

$$\lambda_\tau = (\mathbf{I}_{\beta_{\tau+1}} + \chi_{\tau+1}^T G_\tau^{-1} \chi_{\tau+1})^{-1}, \chi_{\tau+1} = \begin{bmatrix} \mathbf{G}_{\tau+1} \\ \mathbf{U}_{\tau+1} \end{bmatrix},$$

and  $C_{\tau+1}^\theta \in \mathbb{R}^{n \times r}$  is proved analogically. ■

**Proof of Lemma 2.** Consider a DNN with  $h \geq 1$  hidden layers and recall that  $\bar{\psi}^h = [\bar{\psi}_1^h, \bar{\psi}_2^h, \dots, \bar{\psi}_{n_h}^h]^T \in \mathbb{R}^{n_h}$  denotes its last hidden layer and  $\bar{\psi}^o = [\bar{\psi}_1^o, \bar{\psi}_2^o, \dots, \bar{\psi}_r^o]^T \in \mathbb{R}^r$  denotes its output layer. Then  $\bar{\psi}^o$  can be represented by  $\bar{\psi}^h$  as

$$\bar{\psi}_i^o = \bar{\psi}_i^o \left( \sum_{j=1}^{n_h} \theta_{i,j}^h \bar{\psi}_j^h \right), \quad i = 1, 2, \dots, r,$$

where  $\theta^h \in \mathbb{R}^{r \times n_h}$  denotes the weight matrix of the DNN's last hidden layer and  $\bar{\psi}_i^o : \mathbb{R} \rightarrow \mathbb{R}$ ,  $\bar{\psi}_j^h : \mathbb{R} \rightarrow \mathbb{R}$  are generally a nonlinear function chosen by the user.

Define  $\phi = [\phi_1, \phi_2, \dots, \phi_r]^T \in \mathbb{R}^r$  with

$$\phi_i = \sum_{j=1}^{\infty} \theta_{i,j}^h \bar{\psi}_j^h, \quad i = 1, 2, \dots, r,$$

and  $\|\phi\| = 1$ . Let  $\Phi = \begin{bmatrix} \phi \\ u \end{bmatrix}$  with  $u \in \mathbb{R}^m$  denote the control input chosen from the control sequence  $\mathbf{u}$ . Recall the

projection operator from Definition 2. Let  $P := \begin{bmatrix} P_{n_h}^{\mu_1} & \mathbf{0}_{n_h \times m} \\ \mathbf{0}_{m \times n_h} & P_m^{\mu_2} \end{bmatrix}$  with  $\mu_1, \mu_2$  denoting the empirical measurements associated to the  $x_1, x_2, \dots, x_N$  and  $u_1, u_2, \dots, u_N$ , respectively. If Assumption 4 holds, according to Parseval's identity (i.e.,  $\sum_{i=1}^r \sum_{j=1}^{\infty} |\theta_{i,j}^h|^2 = 1$ ), one has

$$\begin{aligned} \|P\Phi - \Phi\|^2 &= \left\| \begin{bmatrix} P_{n_h}^{\mu_1} \phi \\ P_m^{\mu_2} u \end{bmatrix} - \begin{bmatrix} \phi \\ u \end{bmatrix} \right\|^2 \\ &= \left\| \begin{bmatrix} \sum_{j=1}^{n_h} \theta_{1,j}^h \bar{\psi}_j^h - \sum_{j=1}^{\infty} \theta_{1,j}^h \bar{\psi}_j^h \\ \sum_{j=1}^{n_h} \theta_{2,j}^h \bar{\psi}_j^h - \sum_{j=1}^{\infty} \theta_{2,j}^h \bar{\psi}_j^h \\ \vdots \\ \sum_{j=1}^{n_h} \theta_{r,j}^h \bar{\psi}_j^h - \sum_{j=1}^{\infty} \theta_{r,j}^h \bar{\psi}_j^h \\ \mathbf{0}_m \end{bmatrix} \right\|^2 \\ &= \sum_{i=1}^r \sum_{j=n_h+1}^{\infty} |\theta_{i,j}^h|^2 \xrightarrow{n_h \rightarrow \infty} 0. \quad \blacksquare \end{aligned}$$

**Proof of Lemma 3.** Recall the  $L_2$  projection and  $\mathcal{F}_r$  from Definition 2. Before we start the proof, we introduce the following supporting lemma from [5].

**Lemma 4** Let  $\hat{\chi}_k = \begin{bmatrix} x_k \\ u_k \end{bmatrix}$  denote the state of the augmented system and  $\mu_k$  be the empirical measurements with respect to the points  $\hat{\chi}_1, \hat{\chi}_2, \dots, \hat{\chi}_k$  denoted by  $\mu_k = \frac{1}{k} \sum_{i=1}^k \delta_{\hat{\chi}_i}$ , where  $\delta_{\hat{\chi}_i}$  denotes the Dirac measurement in  $\hat{\chi}_i$ . Then for any  $f \in \mathcal{F}_r$ ,

$$K_D f = P_r^{\mu_k} \mathcal{K} f = \arg \min_{g \in \mathcal{F}_r} \|g - \mathcal{K} f\|_{L_2(\mu_k)}.$$

**Remark 7** Lemma 4 shows that the approximated Koopman operator  $K_D$  is the  $L_2$  projection of the Koopman operator  $\mathcal{K}$  in  $\mathcal{F}_r$  associated with the empirical measure supported in samples  $\hat{\chi}_1, \hat{\chi}_2, \dots, \hat{\chi}_k$ .

Then recall  $\Phi, P$  defined in **Proof of Lemma 2** and rewrite  $\Phi$  as  $\Phi = P\Phi + (I - P)\Phi$ . According to Lemma 4, one lets  $K_D := P\mathcal{K}$  be the approximated sequence of Koopman operators which leads to

$$\begin{aligned} \|K_D P\Phi - \mathcal{K}\Phi\| &= \|P\mathcal{K}P\Phi - \mathcal{K}\Phi\| \\ &= \|(P - I)\mathcal{K}P\Phi + \mathcal{K}(P - I)\Phi\| \\ &\leq \|(P - I)\mathcal{K}P\Phi\| + \|\mathcal{K}(P - I)\Phi\| \\ &\leq \|(P - I)\mathcal{K}\Phi\| + \|(P - I)(\mathcal{K}P \\ &\quad - \mathcal{K})\Phi\| + \|\mathcal{K}\| \|(P - I)\Phi\|. \end{aligned} \tag{29}$$

According to Lemma 2, one has

$$\lim_{n_h \rightarrow \infty} \|K_D P\Phi - \mathcal{K}\Phi\| = 0. \quad \blacksquare$$

**Proof of Theorem 1.** Abusing some notations, we first show that the estimation error in (20) is bounded. Recall that given the latest  $\mathcal{B}_\tau$  with  $\{x_{k-1}, u_{k-1}\}$  its latest data point (i.e.,  $x_{k-1} := x_{k_\tau + \beta_\tau}$ ,  $u_{k-1} := u_{k_\tau + \beta_\tau}$ ),  $x_k \in \mathbb{R}^n$  denotes the state of the system of the unknown NTVS evolving from  $x_{k-1} \in \mathbb{R}^n$  and  $u_{k-1} \in \mathbb{R}^m$ .  $\hat{x}_k$  in (21) denotes the estimated state introduced by the proposed method. Here, we extend the estimation error in (20) as

$$\|e_k\| = \|x_k - \hat{x}_k + x_{k-1} - x_{k-1}\|. \quad (30)$$

For any  $\bar{x} \in \mathcal{B}_\tau^x$ ,  $\bar{u} \in \mathcal{B}_\tau^u$  (note that here  $x_{k-1} = \bar{x}_{k-1}$ ,  $u_{k-1} = \bar{u}_{k-1}$  since  $\{x_{k-1}, u_{k-1}\}$  is the observed state-input data point), we introduce  $\epsilon_k$  as the local estimation error induced by the system approximation in (10) given by

$$\epsilon_k = g(\bar{x}_k, \theta_\tau) - (A_\tau g(\bar{x}_{k-1}, \theta_\tau) + B_\tau \bar{u}_{k-1}).$$

Similarly, let  $\bar{\epsilon}_k$  denote the approximation error induced by the minimization of (11) by

$$\bar{\epsilon}_k = \bar{x}_k - C_\tau g(\bar{x}_k, \theta_\tau),$$

which leads to

$$\bar{x}_{k-1} = C_\tau (A_\tau g(\bar{x}_{k-2}, \theta_\tau) + B_\tau \bar{u}_{k-2}) + C_\tau \epsilon_{k-1} + \bar{\epsilon}_{k-1}. \quad (31)$$

By substituting (21) and (31) into (30), we have the following.

$$\begin{aligned} \|e_k\| &= \|C_\tau A_\tau (g(\bar{x}_{k-2}, \theta_\tau) - g(\bar{x}_{k-1}, \theta_\tau)) + C_\tau B_\tau \\ &\quad (\bar{u}_{k-2} - \bar{u}_{k-1}) + C_\tau \epsilon_{k-1} + x_k - \bar{x}_{k-1} + \bar{\epsilon}_{k-1}\|, \\ &\stackrel{(i)}{\leq} \|C_\tau A_\tau (g(\bar{x}_{k-2}, \theta_\tau) - g(\bar{x}_{k-1}, \theta_\tau))\| + \|C_\tau B_\tau \\ &\quad (\bar{u}_{k-2} - \bar{u}_{k-1})\| + \|C_\tau \epsilon_{k-1}\| + \|x_k - \bar{x}_{k-1}\| \\ &\quad + \|\bar{\epsilon}_{k-1}\|, \\ &\stackrel{(ii)}{\leq} \|C_\tau A_\tau\| \|g(\bar{x}_{k-2}, \theta_\tau) - g(\bar{x}_{k-1}, \theta_\tau)\| + \\ &\quad \|C_\tau B_\tau\| \|\bar{u}_{k-2} - \bar{u}_{k-1}\| + \|C_\tau\| \|\epsilon_{k-1}\| + \\ &\quad \|x_k - \bar{x}_{k-1}\| + \|\bar{\epsilon}_{k-1}\|, \end{aligned} \quad (32)$$

where (i) follows the triangle inequality and (ii) is derived by subordnance and submultiplicativity.

For the first two terms of (32), if Assumptions 2-3 hold, one has

$$\|C_\tau A_\tau\| \|g(\bar{x}_{k-2}, \theta_\tau) - g(\bar{x}_{k-1}, \theta_\tau)\| \leq \|C_\tau A_\tau\| \mu_g \mu_x$$

and

$$\|C_\tau B_\tau\| \|\bar{u}_{k-2} - \bar{u}_{k-1}\| \leq \|C_\tau B_\tau\| \mu_u.$$

For writing convenience, one denotes

$$L_a := \|C_\tau A_\tau\| \mu_g \mu_x + \|C_\tau B_\tau\| \mu_u. \quad (33)$$

For the third term of (32), one can derive the error bound of  $\|\epsilon_{k-1}\|$  by backpropagating it from  $k$  to  $k_0 = 0$ . Define the global approximation error in  $\mathcal{B}_\tau$  as

$$\mathcal{E}_k = g(\bar{x}_k, \theta_\tau) - \prod_{i=0}^k A_i g(\bar{x}_0, \theta_0) - \sum_{j=0}^{k-1} \left( \prod_{l=0}^{k-j-1} A_l \right) B_j u_j. \quad (34)$$

The related proof is inspired by the global accumulation rule of  $\epsilon_k$  of time-invariant systems proposed in [20] given by

$$E_k = \sum_{i=0}^{k-1} A^i \epsilon_{k-i}. \quad (35)$$

To achieve the error bound  $\mathcal{E}_k$  in (34), it is necessary to replace  $A$  in (35) with  $A_\tau$  (note that the batch index  $\tau$  is slower than the data point index  $k$ ). For writing convenience, for  $k \in [t_{k_\tau}, t_{k_\tau + \beta_\tau}]$ , define  $k_\tau := t_{k_\tau}$ . Then  $\mathcal{E}_k$  is derived by induction, that is,

- when  $\tau = 1$ ,  $k \in [k_1, k_1 + \beta_1]$ ,

$$\mathcal{E}_k = \sum_{i=0}^{k-k_1-1} A_1^i \epsilon_{k-i} + A_1^{k-k_1-1} \sum_{j=1}^{\beta_0} A_0^j \epsilon_{k_1+1-j}, \quad (36)$$

- when  $\tau > 1, k \in [k_\tau, k_\tau + \beta_\tau]$ ,

$$\mathcal{E}_k = \sum_{i=0}^{k-k_\tau-1} A_\tau^i \epsilon_{k-i} + A_\tau^{k-k_\tau-1} \left( \sum_{j=1}^{\beta_{\tau-1}} A_{\tau-1}^j \epsilon_{k_\tau+1-j} + \left( \sum_{l=1}^{\tau-1} \sum_{m=1}^{\beta_{l-1}} \left( \prod_{n=\tau-1}^l A_n^{\beta_n} \right) A_{l-1}^m \right) \epsilon_{k_l+1-m} \right), \quad (37)$$

- when  $\tau + 1, k \in [k_{\tau+1}, k_{\tau+1} + \beta_{\tau+1}]$ ,

$$\mathcal{E}_k = \sum_{i=0}^{k-k_{\tau+1}-1} A_{\tau+1}^i \epsilon_{k-i} + A_{\tau+1}^{k-k_{\tau+1}-1} \left( \sum_{j=1}^{\beta_\tau} A_\tau^j \epsilon_{k_{\tau+1}+1-j} + \left( \sum_{l=1}^{\tau} \sum_{m=1}^{\beta_{l-1}} \left( \prod_{n=\tau}^l A_n^{\beta_n} \right) A_{l-1}^m \right) \epsilon_{k_l+1-m} \right). \quad (38)$$

According to (36)-(38), the third term of (32) is bounded by

$$\| C_\tau \epsilon_{k-1} \| \leq \| C_\tau \left( \sum_{i=0}^{k-k_\tau-2} A_\tau^i + A_\tau^{k-k_\tau-2} \left( \sum_{j=1}^{\beta_{\tau-1}} A_{\tau-1}^j + \sum_{l=1}^{\tau-1} \sum_{m=1}^{\beta_{l-1}} \left( \prod_{n=\tau-1}^l A_n^{\beta_n} \right) A_{l-1}^m \right) \right) \| L_1.$$

where

$$L_1 = \max_{\substack{\bar{x}_s \in \mathcal{B}_\tau^x, \\ \bar{u}_s \in \mathcal{B}_\tau^u}} \| g(\bar{x}_{s+1}, \theta_\tau) - A_\tau g(\bar{x}_s, \theta_\tau) - B_\tau \bar{u}_s \| . \quad (39)$$

For the last two terms of (32), if Assumption 2 holds, one has

$$\| x_k - \bar{x}_{k-1} \| < \mu_x,$$

and since  $\bar{\epsilon}_{k-1}$  is defined on  $\mathcal{B}_\tau^x$ , one can compute its upper bound by

$$\| \bar{\epsilon}_{k-1} \| \leq L_2 = \max_{\bar{x} \in \mathcal{B}_\tau^x} \| \bar{x} - C_\tau g(\bar{x}, \theta_\tau) \| . \quad (40)$$

To sum up, recall  $L_1$  in (39) and  $L_2$  in (40), let

$$L_b := \| C_\tau \left( \sum_{i=0}^{k-k_\tau-2} A_\tau^i + A_\tau^{k-k_\tau-2} \left( \sum_{j=1}^{\beta_{\tau-1}} A_{\tau-1}^j + \sum_{l=1}^{\tau-1} \sum_{m=1}^{\beta_{l-1}} \left( \prod_{n=\tau-1}^l A_n^{\beta_n} \right) A_{l-1}^m \right) \right) \| L_1 \quad (41)$$

and

$$L_c := \mu_x + L_2, \quad (42)$$

the estimation error  $e_k$  in (30) is upper bounded by

$$\| e_k \| \leq L_a + L_b + L_c. \quad (43)$$

We further reduce the error bound derived in (43) based on Lemmas 2-3. Recall that  $K_D := PK$  in (29) and let

$$\Phi_D^T(\bar{x}_k, \bar{u}_k) := [g(\bar{x}_k, \theta_\tau)^T, \bar{u}_k^T]^T.$$

According to Lemma 2 ( $\lim_{n_h \rightarrow \infty} \Phi_D^\tau = \Phi^\tau$ ) and Lemma 3 ( $\lim_{n_h \rightarrow \infty} K_D^\tau = \mathcal{K}^\tau$ ), by following the Definition of Koopman operator in 1, one has

$$\lim_{n_h \rightarrow \infty} K_D^\tau \Phi_D^\tau(\bar{x}_s, \bar{u}_s) = [\mathcal{K}^\tau \Phi^\tau](\bar{x}_s, \bar{u}_s) = \Phi^\tau(\bar{x}_{s+1}, \bar{u}_{s+1}). \quad (44)$$

Since we are interested in predicting the future values of the system state, we can only keep the first  $r$  rows of  $\Phi_D^\tau(\bar{x}_{s+1}, \bar{u}_{s+1})$  and  $K_D^\tau \Phi_D^\tau(\bar{x}_s, \bar{u}_s)$ . Therefore, we define  $\bar{K}^\tau$  and  $\bar{K}_D^\tau$  as the first  $r$  rows of  $K^\tau$  and  $K_D^\tau$ , respectively, and decompose the matrix  $\bar{K}_D^\tau$  as  $\bar{K}_D^\tau = [A_\tau, B_\tau]$ . Then according to (44), one has

$$\lim_{n_h \rightarrow \infty} L_1 = \max_{\substack{\bar{x}_s \in B_\tau^x, \\ \bar{u}_s \in B_\tau^u}} \|g(\bar{x}_{s+1}, \theta_\tau) - [\bar{K}^\tau \Phi^\tau](\bar{x}_s, \bar{u}_s)\| = 0.$$

Finally, recall  $L_a$  in (33) and  $L_c$  in (42), one has

$$\begin{aligned} \lim_{n_h \rightarrow \infty} \sup \|e_k\| = & (\|C_\tau A_\tau\| \mu_g + 1) \mu_x + \|C_\tau B_\tau\| \mu_u \\ & + \max_{\bar{x} \in B_\tau^x} \|\bar{x} - C_\tau g(\bar{x}, \theta_\tau)\|. \quad \blacksquare \end{aligned}$$

**Proof of Corollary 1.** Recall  $L_b$  in (41). If Assumption 5 holds, by following the properties of triangle inequality and submultiplicativity, one has  $\|\sum_{i=0}^{\beta_\tau} A_\tau^i\| < \beta_\tau$  and  $\|A_\tau^{\beta_\tau}\| < 1$ , which leads to

$$L_b < \|C_\tau\| L_1 (\beta_\tau + \beta_{\tau-1} + \|\sum_{l=1}^{\tau-1} \sum_{m=1}^{\beta_{l-1}} (\prod_{n=\tau-1}^l A_n^{\beta_n}) A_{l-1}^m\|).$$

Following the submultiplicativity, one has  $\lim_{\tau \rightarrow \infty} \|\sum_{l=1}^{\tau-1} \sum_{m=1}^{\beta_{l-1}} (\prod_{n=\tau-1}^l A_n^{\beta_n}) A_{l-1}^m\| = \mu_c$  with  $\mu_c$  a positive constant, which leads to

$$\lim_{\tau \rightarrow \infty} \sup L_b = \|C_\tau\| L_1 (\beta_\tau + \beta_{\tau-1} + \mu_c). \quad (45)$$

By substituting (45) into (43), one can notice that  $\lim_{k \rightarrow \infty} \sup \|e_k\|$  is determined by the minimization performance of (17) and  $\mu_x, \mu_u$ .  $\blacksquare$